The effect of external dynamic loads on the lifetime of rolling element bearings: SEM analysis of raceway surface wear

W. Jacobs[1], R. Boonen[2], P. Sas[2], D. Moens[2]
[1] KU Leuven, Department Mechanical Engineering
Celestijnenlaan 300 B, B-3001, Heverlee, Belgium
e-mail: **William.Jacobs@kuleuven.be**

[2] KU Leuven, Department Mechanical Engineering
Celestijnenlaan 300 B, B-3001, Heverlee, Belgium

Abstract
Accurate prediction of the lifetime of rolling element bearings is a crucial step towards a reliable design of many rotating machines. Recent research emphasises an important influence of external dynamic loads on the lifetime of bearings. The loads can result from structural resonances, gear meshing, etc. Lifetime calculations of bearings are based on the classical ISO 281 standard, neglecting their influence. Inaccurate estimations of the lifetime lead to excessive safety factors during design and unexpected failures during operation. This paper analyses the influence of external dynamic loads using a novel bearing test rig. The test rig allows applying static and dynamic loads on the test bearing in both the radial and axial direction. The effect of radial, axial and combined radial and axial dynamic loads is separately investigated. Microscope images reveal the effect of dynamic loads on wear of the raceway surfaces.

1 Introduction

The importance of research related to failure and damage detection of bearings is self-explanatory. Rolling element bearing failure is one of the foremost causes of breakdown in rotating machinery [1]. Bearings fail prematurely in service due to contamination, poor lubrication, poor fits, misalignments, etc. Motor bearing faults account for more than 40% of the induction motor's failure [2]. Gearbox bearing failure is the top contributor of the wind turbine's downtime [3]. Bearings are cheap, but bearing failure is not. A 4000€ wind turbine bearing replacement can turn into a 200000€ project, even without including the cost of downtime [4].

Lifetime calculations of bearings are based on the ISO 281 standard. For bearings subjected to highly varying loads, recent research emphasises a strong reduction of the actual bearing lifetime w.r.t. the calculated bearing lifetime. For instance in wind turbines, fans and paper making machines, the rolling element bearings are susceptible to failure caused by external machine vibrations. Failure rates of wind turbines approximating three times the failure rate of conventional generators are observed [5]. This is partly due to the unique operational conditions of the bearings, resulting from widely varying wind loads and high vibration levels [6].

Elaborate research on the effect of external dynamic loads on the bearing lifetime is conducted by Gegner and Nierlich [7,8,9,10]. Accelerated lifetime tests under high dynamic load are performed on a series of cylindrical roller bearings. The dynamic load is oriented in the axial direction of the bearing. Axial vibrations lead to sliding motion between surface peaks (also called asperities) of the rolling elements and raceways in contact. Due to the sliding motion, additional tangential loads are introduced on the surface. The tangential loads shift the maximum equivalent stress either closer to or directly on the surface, where residual stresses are built up. Material aging is shifted towards the surface despite almost indentation-free

raceways. Polishing wear shows up as surface induced cracks and material delamination, after only 10^7 revolutions of the test bearing.

The calculated L_{10} bearing life does not incorporate polishing wear due to external dynamic loads. Based on X-ray diffraction (XRD) analysis, a decrease of the L_{10} bearing life of 80% due to the dynamic excitation is estimated. XRD depth profile measurement allows accurate estimation of the stage of material aging. Changes in the width of the α-Fe{211} diffraction line reveal the material strain. The formation of compressive residual stresses is measured based on the material strain. The material residual stresses are derived at different depths of the raceway material.

In other accelerated lifetime tests, Gegner and Nierlich investigate the effect of radial dynamic loads in addition to the axial excitation. Radial vibrations such as oscillating changes of the Hertzian contact pressure can enhance the damaging effect significantly. Rolling element bearings in wind turbine gearboxes normally operate under moderate contact pressures from 1200 to 1600 MPa. Impact events (starting and braking, emergency stops, etc.) introduce short-time peak loads of the maximum contact pressure up to 2500 MPa. The stronger effect of these multi-dimensional vibrations is observed using XRD analysis.

This paper further analyses the effect of external dynamic loads on the bearing lifetime. Firstly, frictional power loss between asperities during dynamic excitation is investigated based on the bearing temperature. The measuments reveal the operational conditions (static loads, dynamic loads and speed) at which polishing wear due to external dynamic loads is expected to be maximal. Secondly, polishing wear is investigated after a series of accelerated lifetime tests under high dynamic load.

The temperature of the bearing and wear of the raceway surfaces are analysed using a novel bearing test rig. The test rig is able to apply a fully controlled multi-axial static and dynamic load on a single test bearing. This unique test rig is designed and constructed in-house. In the current study, a deep groove ball bearing 6302 (designation according to DIN 623) with an outer diameter of 52 mm is mounted. It is lubricated using all-purpose industrial grease, consisting of lithium soap and mineral oil.

The test rig is introduced in section 2. Section 3 describes the analysis of the frictional power loss during dynamic excitation. In section 4, the results of a series of accelerated lifetime tests are reviewed.

2 Bearing test rig

For the study of this paper, a novel bearing test rig is developed. The test rig allows applying an independently controlled load in the radial and axial direction. Furthermore, the load has a static and dynamic component in both directions. The main concept and overview of the test rig are outlined in figure 1. An electric motor drives a shaft through a flexible coupling. The shaft is supported by two bearings, forming a rigid spindle. At the end of the shaft, a third bearing is mounted. This is the test bearing. The load is directly applied on the stationary outer ring of the test bearing. A full review of the test rig can be found in an earlier publication of the authors [11].

Figure 2 gives an overview of the actuator configuration. The static load is generated by four air springs, transferring their force to the bearing housing. Two air springs control the axial force $F_{a,s}$ and two air springs control the radial force $F_{r,s}$. The air springs apply a static force up to 10 kN in each direction. The dynamic load is directly introduced on the bearing housing through the stingers of the electrodynamic shakers: one stinger for the axial direction $F_{a,d}$ and one stinger for the radial direction $F_{r,d}$. The electrodynamic shakers generate a dynamic force in a frequency range from 0 to 5000 Hz with an amplitude up to 1 kN in each direction. In the current study, the excitation resulting from a structural resonance or gear meshing is simulated. The shakers therefore apply a sinusoidally varying load on the bearing with an excitation frequency f_e. The resulting relative motion of the outer ring w.r.t. the inner ring of the test bearing is a sinusoidal displacement with an amplitude A_d and a frequency f_e. This displacement is measured in both the radial and axial direction using capacitive proximity probes [11].

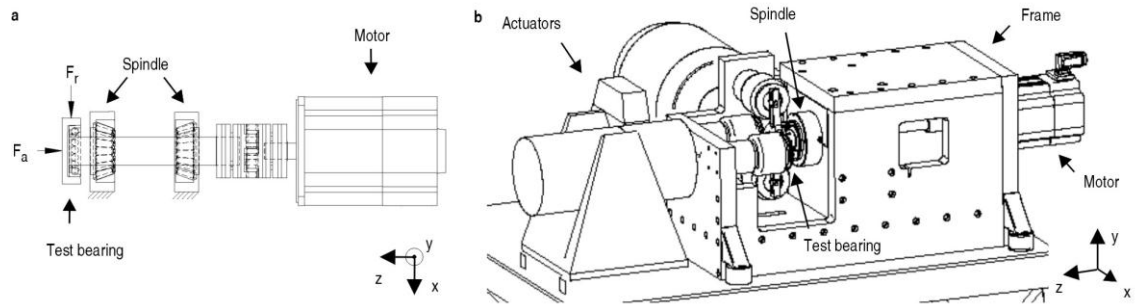

Figure 1: Concept (a) and overview (b) of the presented test rig. The test bearing is mounted on a spindle and driven by an electric motor. The actuators apply a radial force (F_r) and an axial force (F_a) on the test bearing.

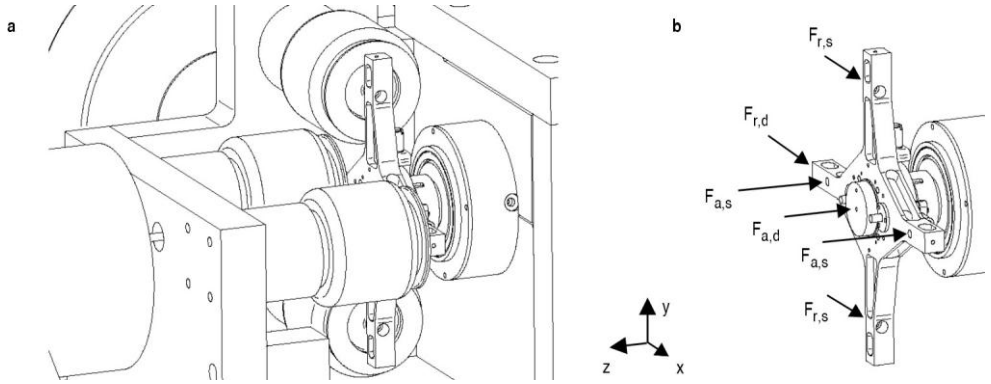

Figure 2: Actuators (a) and their corresponding force vectors (b) of the test rig.

To avoid an uncontrolled and unwanted tilting moment on the bearing, the applied load acts through the centre of the bearing. The static actuators are positioned such that the resulting static force acts through the centre of the bearing. Also, the excited structure, consisting mainly of the housing and sleeve of the test bearing and the upper part of the air springs, is balanced. The centre of gravity of this structure coincides with the centre of the bearing. Therefore, the resulting dynamic force acts through the bearing centre.

3 Frictional power loss under dynamic load

When introducing an external dynamic excitation, the bearing temperature increases. Frictional power loss proportional to the temperature increase is analysed using a thermocouple on the outer ring. This section identifies the heat generation mechanism.

3.1 Thermal analysis of the test bearing

Frictional heat is generated in the contacts of the bearing. A part of this heat is dissipated by conduction through the outer ring and housing and by convection to the environment. The heat transfer from the outer ring to the environment is described by the model of figure 3. The frictional power loss Q expresses the heat transfer rate. The thermal resistance related to the heat transfer through the outer ring is given by the conduction resistance $R_{cond,o}$. The temperature decreases from T_{1o} at the rolling element side to T_{2o} at the housing side. The heat further passes the conduction resistance of the housing $R_{cond,h}$ and the convection resistance R_{conv}. Through convection, the temperature decreases from T_s at the housing surface to T_∞. Such simplified representation is often used to solve steady heat transfer problems. The approach assumes i.e. a constant surface temperature.

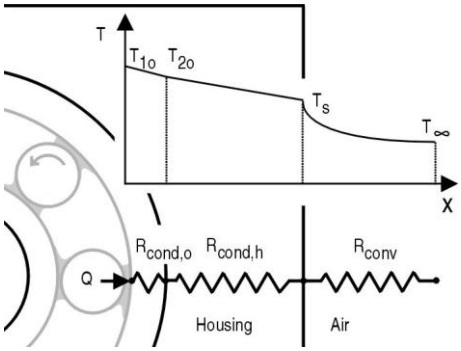

Figure 3: Thermal model of the heat transfer from the outer ring to the environment.

While the conduction resistance $R_{cond,h}$ is independent of the temperature (as stated by Fourier's law of conduction), the convection resistance R_{conv} is not. The dependency should be determined experimentally or numerically and is generally given by the Nusselt number w.r.t. the Grashof number. When introducing an external dynamic excitation while the bearing rotates at 1000 r/min, variations of the outer ring temperature up to 15% are measured. A convection resistance R_{conv} independent of the temperature can be assumed. When assuming a constant convection resistance R_{conv} and a constant temperature of the environment T_{∞}, the frictional power loss Q through the outer ring is proportional to the outer ring temperature T_{2o}.

3.2 Analysis of the frictional power loss

The frictional power loss due to an external excitation is analysed based on an increase of the outer ring temperature T_{2o}. A thermocouple is mounted to the outer ring and located in the loaded zone of the radial load. When changing the static load, dynamic load or rotational speed, the temperature is recorded after the bearing's temperature has reached its stable value. Random temperature fluctuations over time up to 0.5 ˚C are observed after the stable value is reached. Consistent trends of the temperature increase due to an external dynamic excitation are found after repeating the same tests several times.

The effect of a radial, axial and combined radial and axial excitation is analysed. The excitation frequencies correspond to resonance frequencies of the bearing structure, such that high bearing displacements are obtained. The dynamics of the bearing structure are extensively discussed in an earlier publication of the authors [12]. The bearing rotates at 1000 r/min and a 1000 N radial load is applied. The following load cases are separately investigated:

1. A radial sine excitation ($F_{r,d}$ = 35 N and f_e = 540 Hz) is added. The amplitude of the resulting radial displacement equals 6.9 μm. However, no measurable increase of the outer ring temperature is observed.
2. An axial sine excitation ($F_{a,d}$ = 35 N and f_e = 210 Hz) is added. The amplitude of the resulting axial bearing displacement equals 61 μm. After 4 hours, a new stable temperature is reached. The temperature increase due to this dynamic excitation equals 2.7 ˚C.
3. A combined sine excitation in the radial ($F_{r,d}$ = 35 N and f_e = 540 Hz) and axial ($F_{a,d}$ = 35 N and f_e = 210 Hz) direction is added. A similar increase of the outer ring temperature as seen in the second case is measured. No effect of the radial dynamic load is seen.
4. An axial static load of 35 N is added. No measurable increase of the outer ring temperature is observed.

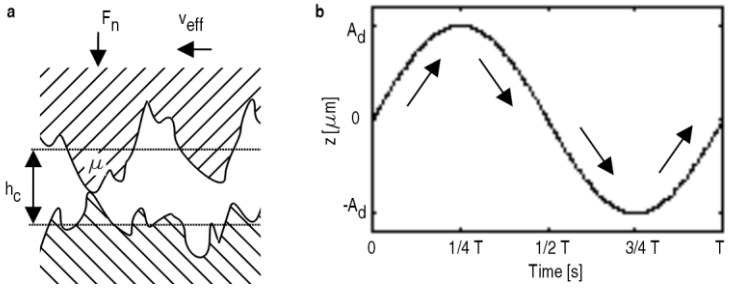

Figure 4: Random metallic contact of asperities (a). The sinusoidal displacement of the outer ring under axial excitation (b).

A significant increase of the bearing temperature is seen when a strong axial excitation is applied. While a lubricant film (with thickness h_c) separates the rolling surfaces, asperities of the rolling element and raceway surfaces make random metallic contact during normal bearing operation. Figure 4a sketches this condition of mixed friction. The axial motion leads to an effective sliding velocity v_{eff} between asperities, while the normal load F_n results from the radial static load. The frictional power loss is related to Coulomb friction between the asperities with a coefficient of friction μ.

3.3 Influence of the operational conditions

The power loss due to ideal Coulomb friction is proportional to the normal load F_n, the effective sliding velocity v_{eff} and the coefficient of friction μ between the surfaces. Variation of the operational conditions (static loads, dynamic loads and speed) experimentally reveals these relations for axial sliding between asperities:

- Variation of the radial static load $F_{r,s}$ shows the effect of the normal load F_n on the power loss. When increasing the radial static load, the normal load in each contact increases (approximately) proportionally. The power loss due to Coulomb friction therefore increases (approximately) proportionally. Figure 5a shows the temperature increase for different levels of the radial static load. A maximum frictional power loss is measured when the radial static load reaches its maximum value.
- Variation of the displacement amplitude A_d shows the effect of the effective sliding velocity v_{eff} on the power loss. During one period, the distance A_d is travelled 4 times (figure 4b). As f_e cycles occur per unit of time, the effective velocity of the outer ring equals 4 x A_d x f_e. When increasing the displacement amplitude, the effective sliding velocity increases proportionally. The power loss due to Coulomb friction therefore increases (approximately) proportionally. Figure 5b shows the temperature increase for different levels of the displacement amplitude. At high levels of the displacement amplitude, the temperature increase veers off the linear trend. This, probably due to the nonlinear motion of the rolling elements w.r.t. the curved raceways during axial excitation. A maximum frictional power loss is measured when the displacement amplitude reaches its maximum value.
- Variation of the rotational speed shows the effect of the coefficient of friction μ on the power loss. When increasing the rotational speed from 0 to 1500 r/min, a lubricant film is formed between the rolling elements and raceways. This film formation is experimentally analysed based on the electrical resistance through the test bearing in an earlier publication of the authors [13]. The mean coefficient of friction, taking into account the friction of asperities in contact and friction of the lubricant film, consequently varies. Figure 5c shows the temperature increase for different levels of the rotational speed. A maximum frictional power loss is measured when the rotational speed reaches 900 r/min.

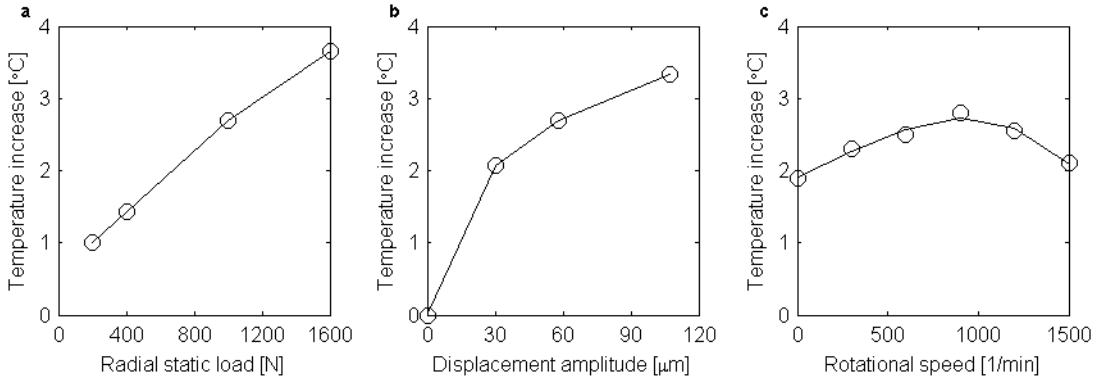

Figure 5: Temperature increase due to frictional power loss under axial dynamic load for different levels of the radial static load (a), displacement amplitude (b) and the rotational speed (c).

4 Surface wear under dynamic load

This section discusses a series of accelerated lifetime tests under high dynamic load, performed using the presented test rig. The test conditions, test duration and test results are described.

4.1 Test conditions

In the study of this paper, accelerated lifetime tests are performed on several deep groove ball bearings. The operational conditions (static loads, dynamic loads and speed) are selected such that the influence of external dynamic loads is expected to be maximal.

4.1.1 Static loads

A maximum frictional power loss is measured when the radial static load reaches its maximum value (section 3.3). Then, the additional tangential loads on the raceway surfaces are maximal and so is the surface wear due to dynamic loads. During the accelerated lifetime tests, a radial static load of 950 N is applied on the test bearing such that the maximum contact pressure on the outer ring equals approximately 2000 MPa. The radial load of 950 N thus represents a high but realistic and common loading condition.

4.1.2 Dynamic loads

To analyse the effect of both a radial and axial excitation, three bearings are dynamically loaded in three different ways:

- A radial dynamic load applied.
- An axial dynamic load applied.
- A radial and axial dynamic load simultaneously applied.

A fourth bearing is tested under the same static load and speed, but without an external dynamic load applied. This bearing serves as a reference when analysing the influence of the dynamic load.

A maximum frictional power loss is measured when the displacement amplitude reaches its maximum value (section 3.3). Then, the additional tangential loads on the raceway surfaces are maximal and so is the surface wear due to dynamic loads. During the accelerated lifetime tests, the amplitude of the dynamic load is controlled and fixed to 50 N in both directions. In order to obtain high displacement amplitudes, the excitation frequencies correspond to resonance frequencies of the bearing structure. The excitation

frequency is set at 536 Hz during radial excitation. The amplitude of the radial bearing displacement then equals 9.8 μm. The excitation frequency is set at 191 Hz during axial excitation. The amplitude of the axial bearing displacement then equals 90.5 μm.

4.1.3 Rotational speed

A maximum frictional power loss is measured when the rotational speed equals 900 r/min (section 3.3). Then, the additional tangential loads on the raceway surfaces are maximal and so is the surface wear due to dynamic loads. During the accelerated lifetime tests, the rotational speed of the bearing is therefore set at 900 r/min.

4.2 Test duration

Based on the static bearing load, an L_{10} bearing life of 1516 days is calculated. Gegner [7] already observes the first surface cracks and material delamination after 10^7 inner ring revolutions of the lifetime tests. An equal amount of inner ring revolutions is chosen for the current tests. This corresponds to a test duration of 7 days of continuous running and 0.5% of the calculated L_{10} life. It should be noted that the dynamic load is applied continuously during the tests. In practical applications, high vibration levels only occur during limited time spans. This, for instance during starting, braking and emergency stops of wind turbines. Also, the operational conditions of the bearing are selected such that surface wear due to sliding between asperities is maximised. The current tests are thus considered being accelerated lifetime tests.

4.3 Test results

After completion of the accelerated lifetime tests, the raceway surfaces of the tested bearings are analysed. The centre of the inner ring raceway surface is investigated using a light optical microscope (LOM) and a scanning electron microscope (SEM). The PHILIPS SEM XL30 FEG uses a secondary electron detector. The beam accelerating voltage is set at 10 kV. In the microscope images of this paper, the overrolling direction equals the vertical direction.

4.3.1 Polishing of the honing structure under axial excitation

When comparing the raceway surface of bearings tested with and without axial dynamic load, polishing of the honing structure under axial excitation is clearly observed. Figure 6 compares the raceway surface of two bearings using a LOM. In figure 7, the same surfaces are analysed under the same magnification using a SEM. The left (a) and right (b) images show the surface of a bearing tested respectively without and with axial dynamic load.

Sharp edges appear as white lines in SEM images, as electrons concentrate in these areas. The rough honing marks of the bearing tested without axial dynamic load are consequently highlighted in these images. The honing marks of the bearing tested with axial dynamic load are polished and thus do not appear. In the LOM images, polishing of the honing structure cannot be seen.

Polishing wear of the surfaces, such as surface cracks and material delamination, is not yet observed. Recalling section 1, Gegner [7] detects this wear after an equal amount of inner ring revolutions when analysing cylindrical roller bearings. Lipless cylindrical roller bearings allow higher axial displacements, such that a higher effect of dynamic loads is expected. The test duration of the current lifetime tests should be increased in order to observe possible polishing wear.

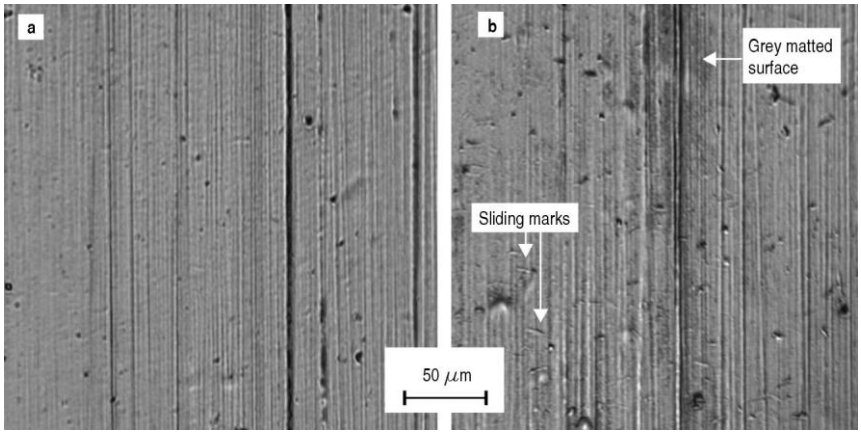

Figure 6: LOM images of inner raceway surface:
test without (a) and with (b) axial dynamic load.

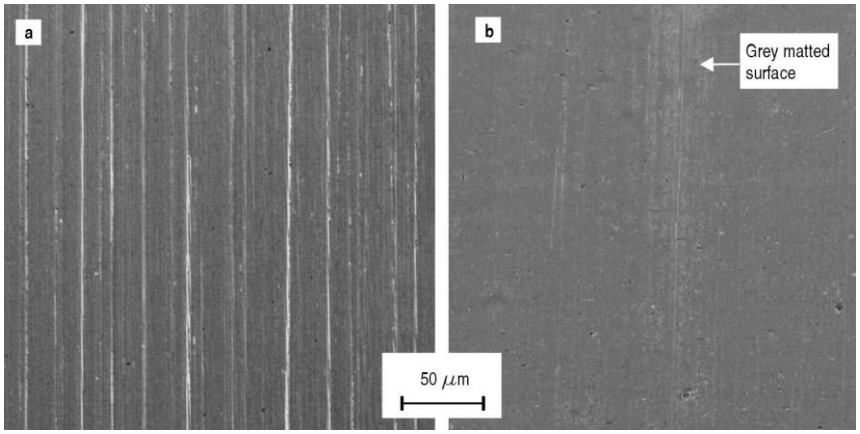

Figure 7: SEM images of inner raceway surface:
test without (a) and with (b) axial dynamic load.

4.3.2 Grey matted surfaces due to arc discharge in the lubricating gap

Both the LOM and SEM images of the tested bearings show grey matted surfaces along the honing marks and indentations. For instance, the honing mark in the middle of figure 6b and 7b is surrounded by these surfaces. As identified at the SKF Material Physics laboratory Schweinfurt, they result from arc discharge in the lubricating gap. The resulting shallow remelted craters of a few micron in diameter and depth cover the raceway surfaces. They are mostly observed along the honing marks and indentations, as the lubricant film formation is worse in these areas.

Arc discharge in the lubricating gap is caused by high frequency electric current passage through the test bearing. It is expected to result from leaking motor currents. Grounding of the spindle shaft is later added to the test rig to eliminate the current passage through the test bearing.

4.3.3 Sliding marks under axial excitation

When comparing the raceway surface of bearings tested with and without axial dynamic load, another difference is noted. The raceway surfaces of the bearings tested under high axial dynamic load are covered by sliding marks (figure 6b). These marks are up to 10 μm long and mainly oriented in the axial direction. Figure 8 shows such a sliding mark for two levels of magnification. Shallow remelted craters resulting from arc discharge are observed at the edges of these marks.

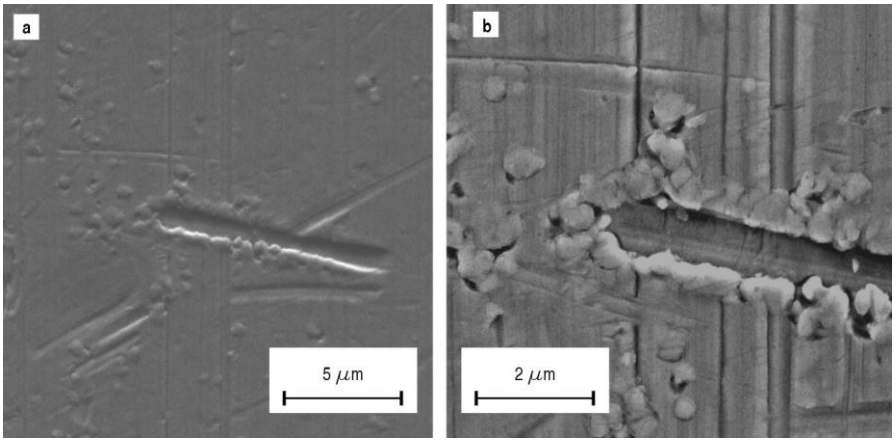

Figure 8: SEM images of a sliding mark:
two levels of magnification (a and b).

The marks are caused by axial sliding of solid particles embedded in the opposing surfaces. While clearly visible on the raceway surfaces, the sliding marks are less important when analysing surface damage. Premature failure under high axial load is caused by polishing wear, rather than the development of these marks.

4.3.4 Radial versus axial excitation

Due to an axial excitation, polishing of the honing structure and the appearance of axial sliding marks are noted. The effect of a radial excitation is not seen:

- When introducing a pure radial dynamic load on a statically loaded bearing, the lubricant film thickness varies at the frequency of excitation. An effect of the excitation on the condition of the raceway surfaces is neither expected nor seen.
- When adding a radial dynamic load to the axial dynamic load of a bearing, an increased effect of the axial excitation is expected. Recalling section 1, a higher Hertzian pressure amplifies the effect of vibration-induced mixed friction. This is not seen in the LOM and SEM images of the current tests. XRD analysis of the raceway surfaces is required for further investigation.

5 Conclusions

This paper experimentally investigates the influence of external dynamic loads on the lifetime of rolling element bearings. Firstly, increased frictional power loss during dynamic excitation is analysed. Secondly, wear of the raceway surfaces after a series of accelerated lifetime tests under high dynamic load is analysed.

Under axial excitation, sliding motion between asperities of the contacting surfaces in the bearing occurs. Based on the temperature increase due to Coulomb friction between asperities, the optimal conditions for accelerated lifetime tests under high axial dynamic load are derived. Accelerated lifetime tests reveal polishing of the raceway honing structure. This polishing is clearly observed on SEM images of the inner raceway after a test duration of only 0.5% of the calculated L_{10} life. When the bearing is further exposed to the high axial dynamic load, polishing wear of the surfaces is expected.

The study promotes further research to analyse surface wear due to external dynamic loads. As a part of future research, longer accelerated lifetime tests will be performed. XRD analysis allows objectifying the occurrence of polishing wear. It will also be used to investigate the influence of increased Hertzian pressure due to an additional radial dynamic load.

Acknowledgements

The authors wish to thank Jürgen Gegner and Wolfgang Nierlich for their helpful and constructive comments during the study on surface wear. The presented research is funded by a Ph.D. grant of the Agency for Innovation by Science and Technology (IWT). Part of the work is performed through the support of the IWT SBO-project Prognostics for Optimal Maintenance.

References

[1] Y. Li, S. Billington, C. Kurfess, T. Danyluk, S. Liang, *Adaptive prognostics for rolling element bearing condition*, Mechanical Systems and Signal Processing, Vol. 13, No. 1, Elsevier (1999), pp. 103-113.

[2] L. Popa, B. Jensen, E. Ritchie, I. Boldea, *Condition monitoring of wind generators*, In *Proceedings of the IAS Annual Meeting, Salt Lake City, USA, 2003 October 12-16*, Salt Lake City (2003), pp. 1839-1846.

[3] H. Link, W. LaCava, J. van Dam, B. McNiff, S. Sheng, R. Wallen, M. McDade, S. Lambert, S. Butterfield, F. Oyague, *Gearbox Reliability Collaborative Project Report: Findings from Phase 1 and Phase 2 Testing*, Technical Report, TP-5000-518852011, NREL (2011).

[4] C. Hatch, *Improved wind turbine condition monitoring using acceleration enveloping*, Orbit, Vol. 61, GE (2004), pp. 58-61.

[5] R. Wood, *Tribology and corrosion aspects of wind turbines*, In *Wind Energy - Challenges for Materials, Mechanics and Surface Science, London, UK, 2010 October 28*, London (2010).

[6] S. Sheng, *Wind Turbine Micropitting Workshop: A Recap*, Technical Report, TP-500-46572, NREL (2010).

[7] J. Gegner, *Tribological aspects of rolling bearing failures*, Tribology - Lubricants and Lubrication, Chapter 2, InTech (2011), pp. 33-94.

[8] J. Gegner, W. Nierlich, *Operational Residual Stress Formation in Vibration-Loaded Rolling Contact*, Advances in X-ray Analysis, Vol. 52, ICDD (2008), pp. 722-731.

[9] J. Gegner, W. Nierlich, *Service Loading Analysis of Wind Turbine Gearbox Rolling Bearings Based on X-Ray Diffraction Residual Stress Measurements*, In *International Conference on Residual Stresses, Garmisch-Partenkirchen, Germany, 2012 October 7-9*, Zurich (2013), pp. 723-732.

[10] W. Nierlich, J. Gegner, *Material Response Bearing Testing under Vibration Loading*, Bearing Steel: Advances in Rolling Contact Fatigue Strength Testing and Related Substitute Technologies, Vol. 9, STP (2011).

[11] W. Jacobs, R. Boonen, P. Sas, D. Moens, *The effect of external dynamic loads on the lifetime of rolling element bearings: accurate measurement of the bearing behaviour*, J. of Physics: Conference Series, Vol. 364, Nr. 1, IOP (2012).

[12] W. Jacobs, R. Boonen, P. Sas, D. Moens, *The influence of the lubricant film on the stiffness and damping characteristics of a deep groove ball bearing*, Mechanical Systems and Signal Processing, Vol. 42, No. 1-2, Elsevier (2014), pp. 335-350.

[13] W. Jacobs, R. Boonen, P. Sas, D. Moens, *Measuring the lubricant film behaviour of rolling element bearings under different operational conditions*, In *Proceedings of the International Congress on Condition Monitoring and Diagnostic Engineering Management, Helsinki, Finland, 2013 June 11-13*, Helsinki (2013).